Applied Geography 57 (2015) 120–132

Contents lists available at ScienceDirect

Applied Geography

journal homepage: www.elsevier.com/locate/apgeog

# Characterization of coastal environment by means of hyper- and multispectral techniques

Andrea Ciampalini [a, *], Ilaria Consoloni [b], Teresa Salvatici [a], Federico Di Traglia [a, b], Francesco Fidolini [a], Giovanni Sarti [b], Sandro Moretti [a]

[a] Earth Sciences Department, University of Firenze, Via La Pira, 4, 50121, Firenze, Italy
[b] Earth Sciences Department, University of Pisa, Via Santa Maria, 53, 56126, Pisa, Italy

ARTICLE INFO

*Article history:*
Available online

*Keywords:*
Coastal morphology
Multispectral
Hyperspectral
Rip current
Image classification

ABSTRACT

The management of the coastal environment is a complex issue, which needs for appropriate methodologies. Erosional processes and longshore currents present in the submerged beach represent a serious danger for both people and human infrastructures. A proper integration between traditional and innovative techniques can help in the characterization and management of the beach environment. Several different multispectral and hyperspectral techniques were used to retrieve information about the hydro and morphodynamic settings of the Pisa province coast (Tuscany, Italy). Results were validated using about 130 samples collected along the study area, between the mouths of the Serchio river and the Scolmatore canal. The composition of sand samples was evaluated by means of petrographic microscopy and grain size analyses. The same samples were analyzed using an Analytical Spectral Device (ASD) Fieldspec. The obtained sediment spectral library was used to evaluate the differences in mineralogical composition, which can be related to different source areas. Results coming from spectroscopy were compared to those obtained from the petrographic and grain size analysis. Furthermore a multispectral aerial image was used to evaluate sediment distribution along the submerged beach, to map the geomorphic features and to detect the presence of longshore and rip currents. This works suggests that optical remote sensing technique can be profitably used in order to reduce the need for expensive and time consuming conventional analysis.



## Introduction

Coastal zones are very complex and dynamic environments, naturally subjected to recurring morphodynamics changes. However, due to the intensification of human-induced pressure the rate of change is increasing. The management and conservation of coastal areas are crucial, especially in areas where humans are present (Mc Kenna, O'Hagan, Power, Macleod, & Cooper, 2007; Stojanovic & Ballinger, 2009; Zacarias, Williams, & Newton, 2011). Understanding the natural processes characterizing the coastal zones and influencing their evolution is a key point for a proper territory management and planning (Dharmaratne & Braithwaite, 1998; El Mrini, Maanan, Anthony, &Taaouati, 2012; Manning, Wang, Valliere, Lawson, & Newman, 2002). Beaches represent a substantial source of income for their touristic attractive. It is worth noting that beaches are frequented by tens of millions of people worldwide (Lushine, 1991). This amount, combined with the risks related to the hydrodynamic setting, makes beaches locations with a high level of public risk. Among the hazards related to beaches, surf zone processes and beach morphology play an important role (Short & Hogan, 1994). The recognition of these hazards is fundamental to plan a correct management of the coast. One of the most common hazardous processes is constituted by rip currents, which act in the surf zone (Dalrymple, MacMahan, Reniers, & Nelko, 2011; Shaw et al., 2014; Short & Hogan, 1994). A prompt detection of this kind of currents, representing a lethal natural hazard, sensibly increases the beach safety level.

The understanding of the hydrodynamic conditions present along the shore is an important issue not only for people safety but also to protect the coastal environment from erosive processes, which lead economic loss in term of damages to properties and structures.

* Corresponding author. Tel.: +39 055 275748.
*E-mail address:* andrea.ciampalini@unifi.it (A. Ciampalini).

http://dx.doi.org/10.1016/j.apgeog.2014.12.024

A proper management plan of a coastal area must necessarily consider the dynamic processes responsible of the erosion and/or sediment distribution along the shore.

Coastal areas, characterized by the presence of several river mouths, are natural laboratories where the spatial and temporal variability of sediments distribution can be detected. River input of freshwater and/or flood events represent controlling factors on the dispersion and sedimentation dynamics (Kuenzer, van Beijima, Gessner, & Dech, 2014; Small et al., 2009). Several techniques were used and proposed to study the dynamic nature of coastal systems, especially for the determination of changing in shorelines, erosion, and deposition due to sediment transport (Anil Ari, Yüksel, ÖzkanÇevic, Güler, & YalçinerBayram, 2007; Baily & Nowel, 1996; Bertoni, Sarti, Benelli, Pozzebon, & Raguseo, 2010). The composition of clastic sediments is generally characterized by its physical features, chemical composition and petrographic composition (texture and mineralogy).The study of the compositional and textural variability of sediments provides information on the evolution of geography, climate, tectonics and lithology of the sediment source areas and on the dispersal pattern of sediments along the coast (Borges & Huh, 2007). The provenance of littoral sands can be studied though a variety of methods, including petrographic analysis, whole rock and mineral chemistry and radiometric dating. Usually these conventional methods are time consuming and expensive.

In contrast, remote sensing techniques represent inexpensive and fast methods and they are extensively used to monitor the coastal environment and the reflectance properties of sediments (Holman & Haller, 2013; Liu, Islam, & Gao, 2003; Power, Holman, & Baldock, 2011; Small et al., 2009; Teodoro, Pais-Barbosa, Gonçalves, Veloso-Gomes, Taveira-Pinto, 2011; Teodoro, Pais-Barbosa, Veloso-Gomes, & Taveire-Pinto, 2009; Xu et al., 2014). The sediment reflectance spectrum is strongly affected by its lithologic and/or mineralogic composition, grain size distribution and moisture. Furthermore, remote sensed (space-borne and air-borne) images can be suitably used to retrieve and map water characteristics (turbidity, water depth, quality, presence of algae), because these features affect the water optical properties (Liew, Chang, & Kwoh, 2012). Thus these techniques can be profitably used in the management of coastal environments, providing several useful information over wide areas.

The aim of this research is to evaluate remote sensing techniques to identify physic, morphologic and hydrodynamic features which characterize the coastal environment affected by erosive phenomena. Both traditional (grain size and petrographic analysis) and innovative (hyperspectral and multispectral) techniques were used and evaluated in order to provide suitable tools for the management of the coastal environment.

## The study area

The study area, about 26 km long and it is comprised between the Serchio River and the Scolmatore canal outlets (Fig. 1). It belongs to the physiographic unit extending from Punta Bianca to the north and to the Livornesi Mountains to the south, covering a distance of about 70 km (Bertoni & Sarti, 2011). The entire coastal zone is characterized by an elevated anthropic pressure with the exception of the area comprised between the Arno River and La Bufalina (Fig. 1), which falls in the Regional park of Massaciuccoli-San Rossore. The coastal dune systems are mainly preserved within the park area. Three harbors (Fig. 1, Marina di Carrara, Viareggio and Marina di Pisa) strongly interfere with the littoral sedimentary drift triggering erosive processes or producing sandy accumulation down or up drift of the port respectively.

The coast is characterized by sandy beaches faced a wide coastal plain formed by Late Quaternary deposits and fed, from north to south by the Magra, the Serchio and the Arno rivers. The last two, and particularly the Arno river, feed the Pisa shoreline, even if in an insufficient way (Cipriani, Ferri, Iannotta, Paolieri, & Pranzini, 2001). Since Etruscan and Roman times, the Arno river delta progradation took place until the beginning of the second half of the nineteenth century, when erosive processes began (Amorosi, Rossi, & Sarti, Mattei, 2013). The degradation of the Arno river delta apex was induced by several factors (reclamation works, harbors, jetties, sandpits, river dams), which strongly changed the sedimentary budget (Pranzini, 1983; Rapetti & Vittorini, 1974). In particular, the retreat of the shoreline located north of the Arno river mouth exceeded 1000 m in less than 150 years and involved the S. Rossore beach (Fig. 1). To the south, the retreat was limited to approximately 300 m, due to the construction of protection structures (Aminti & Pranzini, 2000; Pranzini, 1989). This particular framework modified through time the natural sediment distribution along the coast modifying the natural shore feeding processes. Shore protections at Marina di Pisa were recently enhanced also by the creation of artificial gravel beaches, which allowed the reduction of invasive approaches to coastal defense and a better exploitation of the shore from a touristic point of view (Bertoni et al., 2010; Bertoni, Sarti, Benelli, Pozzebon, & Raguseo, 2012; Bertoni et al., 2013).

The study area is characterized by a littoral drift (Fig. 1) directed to the north between the Arno river outlet and Forte dei Marmi and to the south between the Arno River and the village of Calambrone, which represents a convergence zone (Aiello et al., 1976; Gandolfi & Paganelli, 1975; Pranzini, 2004).

The climatic setting is dominated by westerly winds, which usually generate seasonal mild storms, whereas southwesterly winds show the highest velocities causing the most strongest and destructive storms (Bertoni & Sarti, 2011). Tidal influence is almost negligible, reaching a maximum excursion of 30 cm (Cipriani et al., 2001).

## Methodology

### *In situ analysis*

Sampling sites are located along 50 transects arranged perpendicular to the coast (Fig. 2). For each site about 1 kg of sediment was collected. Sample positions were located with a differential GPS receiver. Samples were systematically collected at: −9/−10 m (A); −7/−8 m (B); −5/−6 m (C); −4 m (D); −3 m (E); −2 m (F); −1 m (G); swash zone (H); backshore 1 m (K) and 2 m (L). A subset of 70 samples was chosen for a preliminary analysis. Samples were dried and split. A fraction of each sample was used for petrographic and grain size analyses. The organic fraction was removed using hydrogen peroxide. Samples for petrographic analysis were sieved considering only the fraction between 2 mm and 63 μm. The petrographic analysis was performed following the Gazzi-Dickinson method (Dickinson, 1970; Gazzi, 1966; Ingersoll et al., 1984) using 6 classes: quartz; feldspar; plagioclase; lithic grains; mica and carbonates (Dickinson & Suckzek, 1979; Graham, Ingersoll, & Dickinson, 1976; Zuffa, 1980, 1985). For the grain size analysis, 7 classes were defined: gravel (>2 mm); very coarse sand (1–2 mm); coarse sand (0.5–1 mm); medium sand (0.25–0.5 mm); fine sand (125–250 μm); very fine sand (62.5–125 μm) and silt and clay (<62.5 μm).

### *Hyperspectral analysis*

An Analytical Spectral Device (ASD) Fieldspec spectroradiometer was used to collect the samples spectra. This sensor measures reflectance in 3–10 nm bandwidths over the

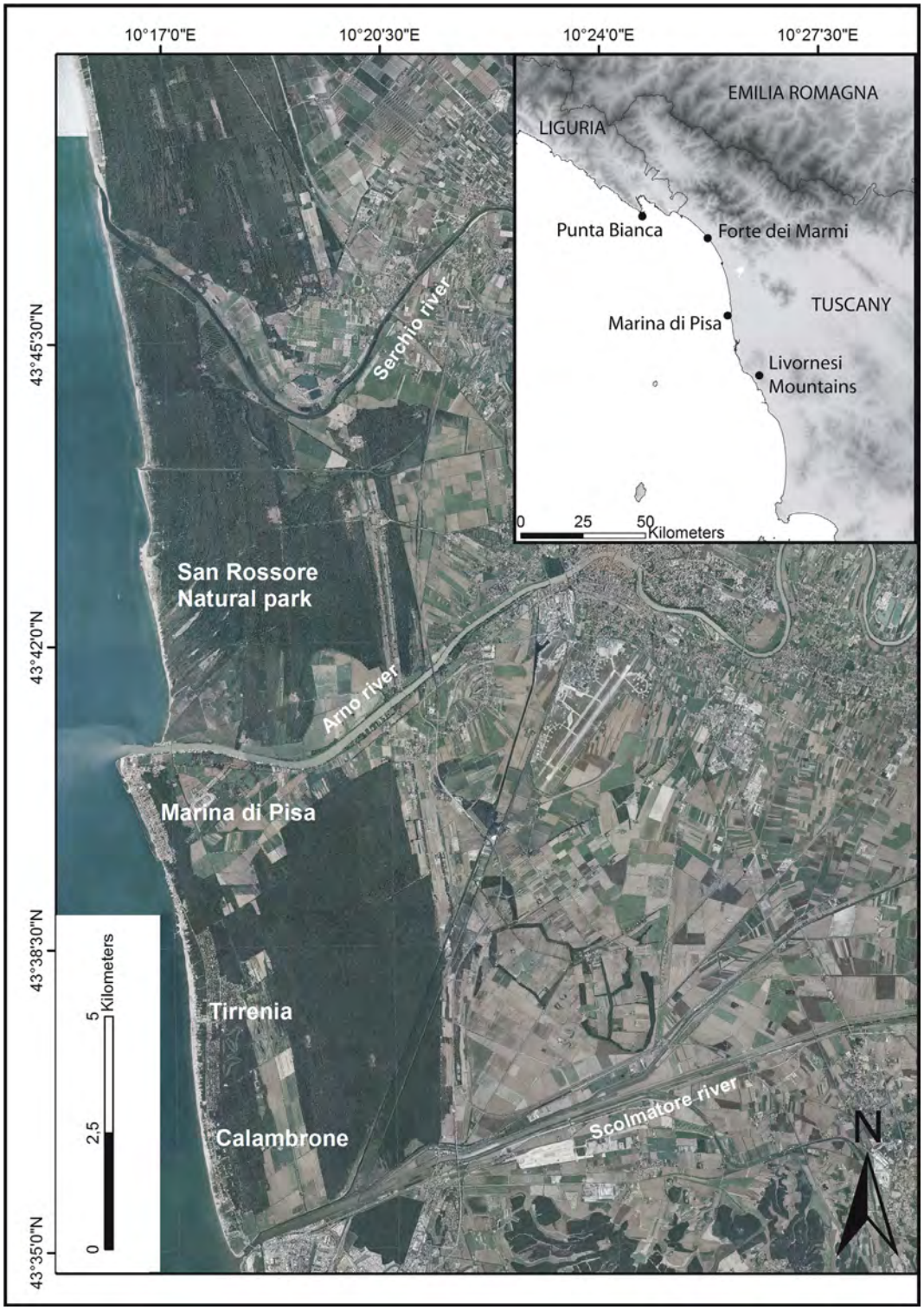


**Fig. 1.** Location of the study area.

350–2500 nm range. The control of the irradiance conditions was assured using a nadir viewing set-up composed of two halogen tungsten lamps (24 V; 70 W) located 60 cm laterally to the samples and inclined at 45°. The distance between the sample and the optic fiber was 7 cm with a table-projected field of view having a diameter of about 3.5 cm. Four measurements were collected and averaged for each sample, which was placed on a watch glass and smoothed by vibration. Reference measurements on the Spectralon panel were acquired systematically every three samples. The spectra acquired for each sample were averaged using the ASD ViewSpec Pro using the splice correction in order to avoid the presence of steps (Garfagnoli, Ciampalini, Moretti, Chiarantini, & Vettori, 2013; Garfagnoli, Martelloni, Ciampalini, Innocenti, & Moretti, 2013). The principal component analysis (PCA) was applied to the spectral dataset. This mathematical procedure is largely used in environmental science and biological applications,

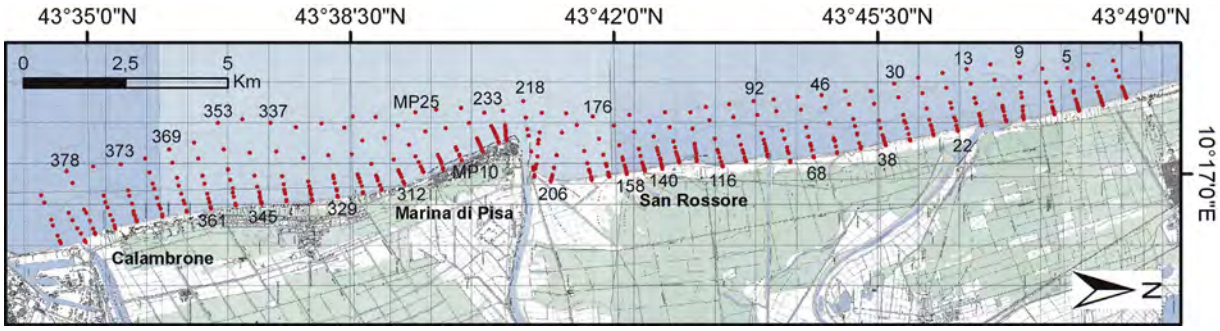


**Fig. 2.** Location of sampling sites along the investigated coastal area. Numbers correspond with some of the analyzed transects.

**Table 1**
Wavelength of the Daedalus spectral bands.

| Band | Wavelength (μm) |
|---|---|
| 1 | 0.43–0.45 |
| 2 | 0.48–0.50 |
| 3 | 0.50–0.52 |
| 4 | 0.52–0.54 |
| 5 | 0.54–0.56 |
| 6 | 0.56–0.58 |
| 7 | 0.58–0.61 |
| 8 | 0.61–0.64 |
| 9 | 0.65–0.68 |
| 10 | 0.68–0.72 |
| 11 | 0.72–0.78 |
| 12 | 0.78–0.84 |
| 13 | 0.84–0.92 |
| 14 | 1.55–1.75 |
| 15 | 2.08–2.35 |
| 16 | 8.5–12.5 |

as a tool for exploratory data analysis and for making predictive models (Abdi & Williams, 2010; Ciampalini, Consoloni, & Sarti, 2011; Ciampalini, Garfagnoli, Antonielli, Moretti, & Righini, 2013; Shaw, 2003). The main purpose of the PCA is to reduce the dimensionality of the original dataset, represented by an n-dimensional space (where n is the number of variables or experimental results), into a few principal components (PC), derived as a linear combination of the original variables, which concomitantly retain the maximum percentage of original information contained in the data set (Khaleghi, Ranijbar, Shahabpour, & Honarmand, 2014; Raiber et al., 2012; Winter, Mallroy, Allen, & Rosenberry, 2000). The new space is defined by the eigenvectors of the data variance–covariance matrix. The resulting PC can be used to project the originally multidimensional data into only a two- or three dimensional space, which is called a score plot (Brenton, 2003). Even without specific knowledge of statistical implications, these plots enable a rapid and direct evaluation of similarities, differences and groupings among the original samples. As a matter of fact, since patterns can be hard to find in data of high dimension, PCA is a powerful data analysis instrument, which reduces the number of dimensions, without much loss of information. This technique was applied to the petrographic classes, to the grain size classes and to the ASD laboratory spectra of sand samples. The first two principal components were then plotted against each other in a scatterplot. Results coming the PCA using the three different datasets are compared in order to establish possible correlations among them (see Table 1).

*Multispectral analysis*

The multispectral analysis of the study area was performed using imagery of DAEDALUS Airborne Thematic Mapper (ATM-2) (Fig. 3), which is a passive multispectral airborne sensor, designed by AGEA/TELAER STA©, that measures the electromagnetic radiance reflected or emitted from the Earth surface. Daedalus acquires using 16 spectral bands in the VIS, NIR, SWIR and LWIR (Table 2) with an instantaneous field of view of 1.25 mrad. The sensor is equipped with a roll, pitch, heading and location with GPS/INS subsystems for the images spatial correction, geo-referentiation and ortho-rectification. Data are stored using a solid state disk drive. The acquisition flight started at the 10:28 am and ended at the 10:34 am of the 10 August 2012. The pixel resolution was 1.3 m considering a height of flight of 1069 m. The flight path was approximately 2.5 km wide and 17 km long and it includes the area located between Marina di Pisa and the Serchio river outlet. The raw data were radiometrically corrected into at-sensor radiance values and then corrected into at-surface reflectance values considering the influence of the atmosphere, solar illumination, sensor viewing and terrain geometries.

The reflectance image was used to evaluate the usefulness of different spectral pixel-based classification methods. These kind of

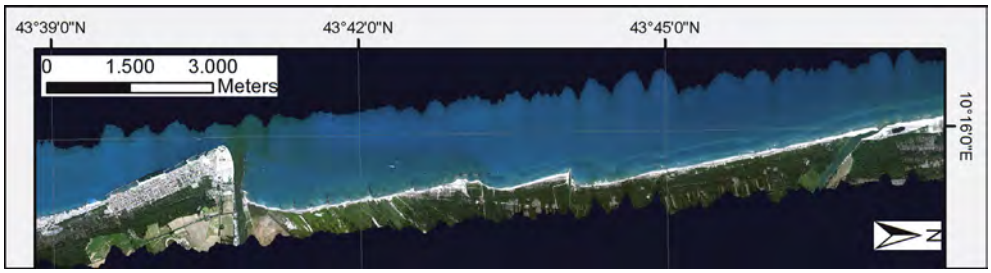


**Fig. 3.** True color image in RGB mode (8,5,2) of the study area acquired using Daedalus. (For interpretation of the references to color in this figure legend, the reader is referred to the web version of this article.)

**Table 2**
Classification accuracy for the supervised classification algorithms.

| | OA | Kc |
|---|---|---|
| Parallelepiped | 89.44 | 0.87 |
| Minimum distance | 97.87 | 0.97 |
| Maximum likelihood | 99.91 | 0.99 |
| Spectral angle mapper | 50.79 | 0.46 |

classifications uses only the available spectral information (Li & Chen, 2005; Pu & Bell, 2013; Teodoro et al., 2009, 2011). Based on its spectral properties, each pixel is labeled independently from the neighboring areas as a given land cover class or geomorphic typology. Such approach is usually termed "pixel-oriented". Four different supervised classification algorithms were tested using only the spectral information. In details, the available image was elaborated using the following supervised classifications: (i) parallelepiped, (ii) minimum distance, (iii) maximum likelihood (Richards, 1999, p. 240) and the (iv) spectral angle mapper (Kruse et al., 1993). The classification was performed considering eleven classes on the base of the elements recognized within the image and verified from field inspection: (1) open sea, (2) crescentic bar, (3) breaking zone, (4) emerged beach, (5) bare soil, (6) pinewood, (7) fresh water, (8) brushland, (9) cultivated field, (10) roofs and (11) gravel beach. Training samples were selected for each considered class using dedicated region of interests (ROI). Each ROI, corresponding to a polygon, includes 200 pixels which were used to define the typical spectral signature of each class. The obtained results were evaluated both through a visual inspection and using a confusion matrix. The latter method allows to quantitatively assess statistically how pixels were effectively grouped into the correct feature class (Teodoro et al., 2011). The accuracy of each used algorithms was measured by the use of two different indexes, which are the results of the confusion matrix: the overall accuracy (OA, Smits, Dellepiane, & Schowengerdt, 1999) and the Kappa coefficient (Kc, Congalton & Mead, 1983; Stehman, 1996). The accuracy of classification was assessed by a set of 2200 points sampled using the stratified random sampling (Abd El-Kawy, Rød, Ismail, & Suliman, 2011; Rozenstein & Karnieli, 2011). For each class 200 points were randomly selected and projected on the Daedalus images in true colors. Furthermore the Principal Component Analysis was also applied to the multispectral image to identifying hydrodynamic forms. This technique is used to compress the multispectral dataset by calculating a new coordinate system. The multispectral dataset is composed by several correlated bands, which are transformed into new uncorrelated components called principal components (Loughlin, 1991). Each PCs image can be singularly analyzed or they can be used to produce false color composite (Chauvaud, Bouchon, & Maniere, 1998; Ciampalini, Garfagnoli, Antonielli, Del Ventisette, & Moretti, 2012, 2013; Teodoro et al., 2011).

## Results

### *In-situ and hyperspectral analysis*

A preliminary petrographic composition analysis of the collected samples was performed using a subset of the available samples. 27 samples collected at −1 m depth were plotted in three diagrams: Q(Quartz)-F(Feldspar)-L(Lithic grains); Q-F + L-C(carbonates) and Q-K-P (Fig. 4A). Samples are distributed according to two main compositional groups (Fig. 4): the first includes the samples located between the northern boundary of the study area and the village of Calambrone (samples 5 to 345 in Fig. 4A), while the second spans from the town of Calambrone to the southern limit of the Pisa Province (samples 353 to 378 in Fig. 4A). All the samples can be classified as litho-feldspatic sands. The discriminant factor between the two groups is represented by the quartz content which is higher for the samples collected north of Tirrenia.

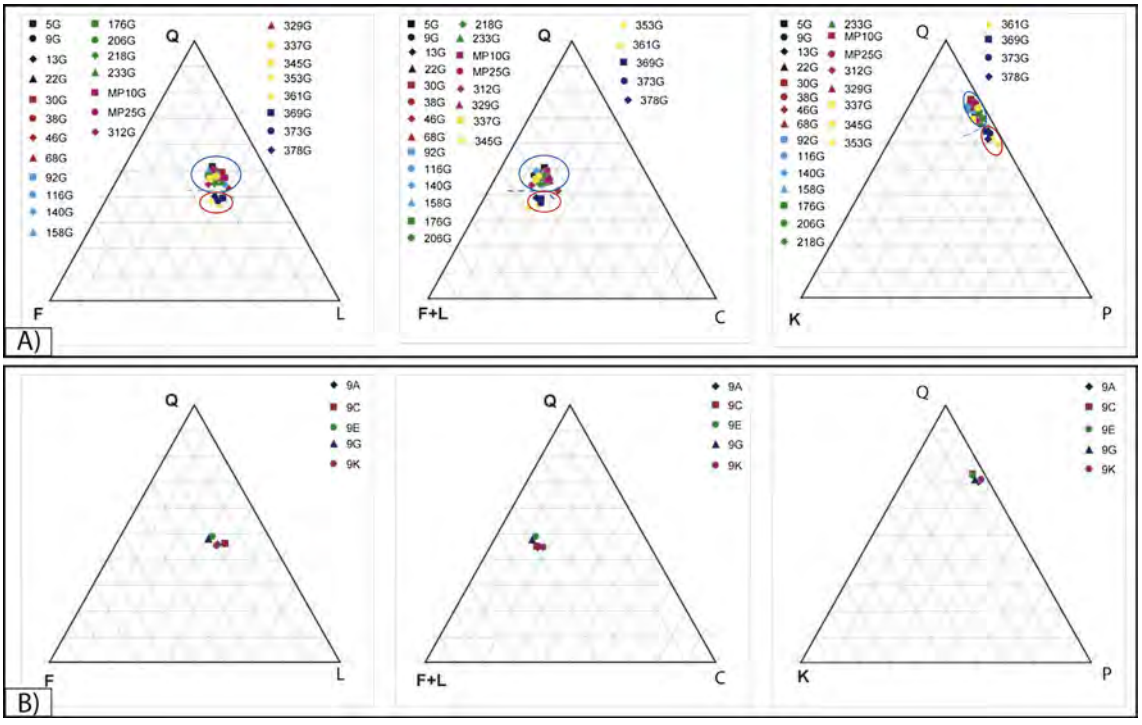


**Fig. 4.** A) Ternary diagrams (Q-F-L; Q-F + L-C and Q-K-P) for the samples collected at −1 m depth. The sample identification number (from 5 to 378) increases from north to south. The dashed line represents the boundary between the two identified group. B): Ternary diagram for the samples collected along transect 9 located in the northern sector of the study area close to the Serchio River outlet.

The compositional variations related to depth were investigated, considering the samples collected to −9, −5, −3, −1, and +1 m depth. Three transects, orthogonal to the coastline, were selected (9, 337 and 373). No evidences of compositional variations were recognized along the transects (Fig. 4B).

The percentage of each grain size class, measured for all the available collected samples, was interpolated by means of the Inverse Distance Weight (IDW) in ArcGIS to highlight the spatial distribution of the considered classes (as proposed Molinaroli et al., 2014). The main factor affecting the accuracy of IDW is the value of the power parameter (Isaaks & Srivastava, 1989), which in our case was set at to a value of 2.

The obtained maps show that the southern sector of the study area (Calambrone) is characterized by the presence of the higher percentages of gravel deposits (Fig. 5A). Also in correspondence with the artificial gravel beaches of Marina di Pisa, an area where gravel deposits represent a consistent fraction is detected. Fig. 5B and C highlight that the proximal submerged beach is characterized by higher percentages of medium sands, whereas the distal area is dominated by fine sands sediments. Fig. 5B and C shows a clear inversion between areas dominated by fine sands and medium sands. Very fine sands and silts reach the highest percentages offshore the Calambrone beach (Fig. 5D).

The PCA on the three datasets (petrography, grain size, spectral data) was performed with SIM-CA P+ software by Umetrics, using 131 observations and 2151 variables. In each case, a three component model was realized after no transformation of variables and mean centering for the spectral dataset, linear transformation and mean centering for the grain size dataset and negative logarithm transformation and unit variance filter for the petrographic dataset. For all the three models (petrography, grain size and spectral data), the first two components explain more than the 90% of the dataset variance and represent the largest differences between the groups of samples. The PCA performed on the petrographic dataset highlights a recognizable cluster formed by samples collected in the southern sector of the study area (black dots in Fig. 6A).

Regarding the grain size dataset (Fig. 6B), the scatter plot of the first two principal components highlights the presence of three groups. Samples collected at −9/10 m depth (A) are grouped and clearly separated from samples collected at −1 m (G) and 1 m (K).

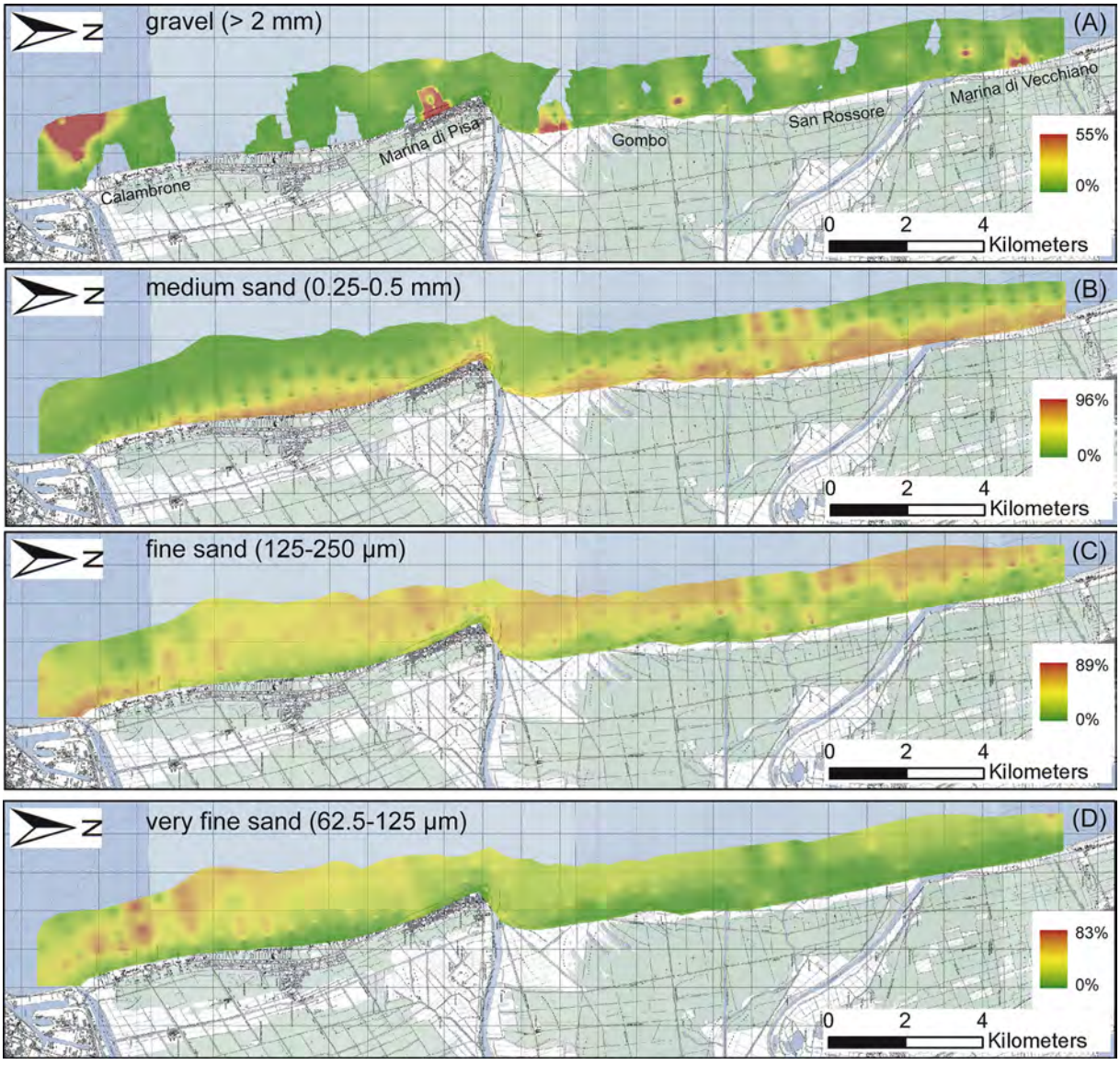


**Fig. 5.** Maps of the percentages of four different grain size classes: gravel (A); medium sands (B); fine sands (C) and very fine sands (D).

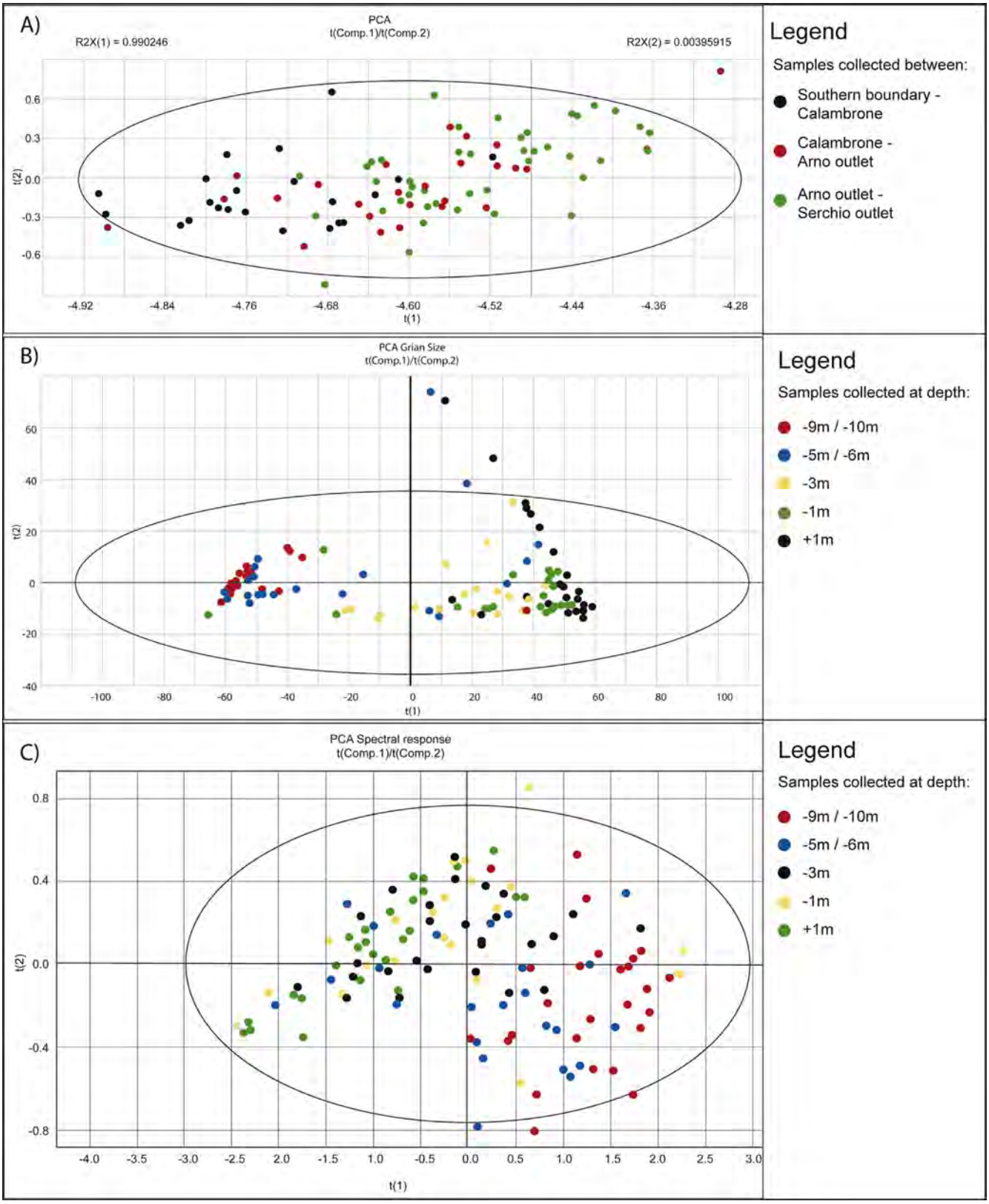


**Fig. 6.** Principal Component graphs. A) Petrography: scatter plot of the first two principal component scores of the petrographic dataset. (Black: samples collected between the southern limit of the study area and the Calambrone village; red: between the Calambrone village and the Arno river outlet; green: between the Arno and Serchio river outlets). B) Grain size: scatter plot of the first two principal component scores. Red samples A (−9/−10 m); blue sample C (−5/−6 m); yellow samples E (−3 m); green samples G (−1 m) and black sample K (1 m). C) Spectral response; scatter plot of the first two principal component scores related to the spectral dataset. Red samples A (−9/−10 m); blue sample C (−5/−6 m); black sample E (−3 m); yellow samples G (−1 m) and green samples K (1 m). The circles represent the 90% of the variance. (For interpretation of the references to color in this figure legend, the reader is referred to the web version of this article.)

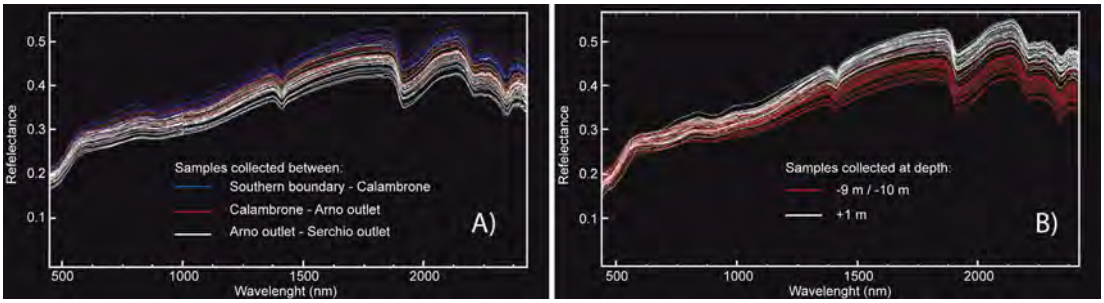


**Fig. 7.** A) Distribution of the spectra of the collected samples at +1 m depth (K). (Blue: samples collected between the southern limit of the study area and the Calambrone village; red: between the Calambrone village and the Arno river outlet; white: between the Arno and Serchio river outlets). B) Distribution of the spectra of the collected samples. Samples K (1 m) are in red and samples A (−9/−10 m) in white. (For interpretation of the references to color in this figure legend, the reader is referred to the web version of this article.)

Most of the samples collected at −5/6 m (C) depth are grouped together, but a part of them are scattered. The model shows that the grouping is mostly affected by the variables: very coarse sands, coarse sands, medium sands and fine sands.

Concerning the spectral properties, in the first two PC score plot (Fig. 6C), samples A and K are located in separated areas (prevalently the first and the fourth quarters for samples K and mainly the second and the third quarters for samples A).

The same grouping patterns are highlighted by the spectral characteristics (Fig. 7). Spectra samples were plotted considering the single bathymetry (+1 m). Samples are grouped considering their location. Southern samples show higher reflectance; on the contrary samples collected north to the Arno river show the lowest reflectance values.

Among the samples collecting at different depth, K (1 m) (Fig. 10) and A (−9/−10 m) show an interesting distribution where the deepest samples show higher reflectance with respect to the others.

*Multispectral analysis*

The supervised classification was applied using four different algorithms in ENVI 5.1: (i) Parallelepiped, (ii) Minimum distance, (iii) Maximum likelihood and (iv) Spectral angle mapper. From a statistical point o view all the used supervised classification algorithms present very good performance but the spectral angle mapper (Table 2).

The Parallelepiped classification (Fig. 8) shows very good results especially for the identification and mapping of the morphological features of the submerged beach and for the detection of the longshore and rip currents directions. The spatial distribution of the crescentic bar, which usually forms after a storm event, is clearly highlighted in green (in web version) (Fig. 8) in the area between the Arno and the Serchio river outlets. The shape and the distribution of the classes “breaking zone” and “crescentic bar” allow to define the direction of the rip currents present along the area located north of the Arno river outlet (Fig. 8 B and C) and to highlight the areas more affected by erosional phenomena.

Results obtained using the Minimum distance algorithm show an improvement considering both the OA and the Kc indexes (Table 2). This algorithm can classify all the image pixels; on the contrary the parallelepiped algorithm presents 69.95% of unclassified pixels. Also in this case the classification highlights several interesting elements of the submerged beach (Fig. 9). The crescentic bar is clearly delineated as well as the presence of some areas affected by rip currents. In particular in the northern part of the study area a rip current is clearly detected in correspondence with a bath (Fig. 9B). In the central part the effect of some breakwaters on the direction of the currents can be evaluated (Fig. 9C).

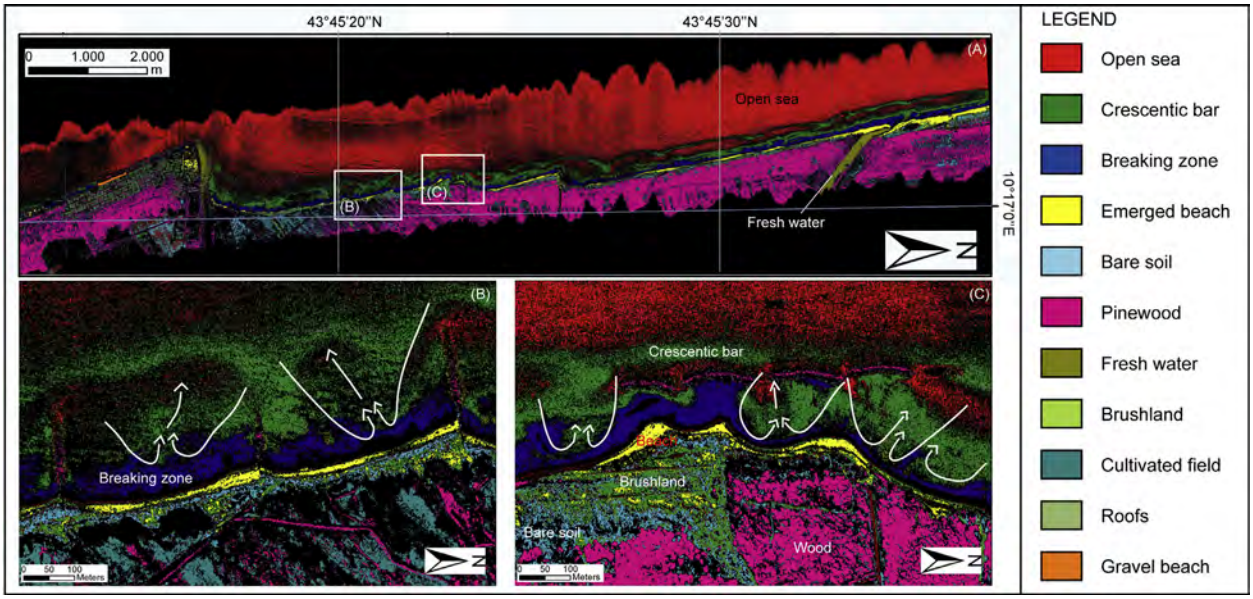


**Fig. 8.** Results of the parallelepiped classification algorithm applied to the Daedalus ATM-2 image (A) and two zoom where the hypothesized rip and longshore currents direction are reported.

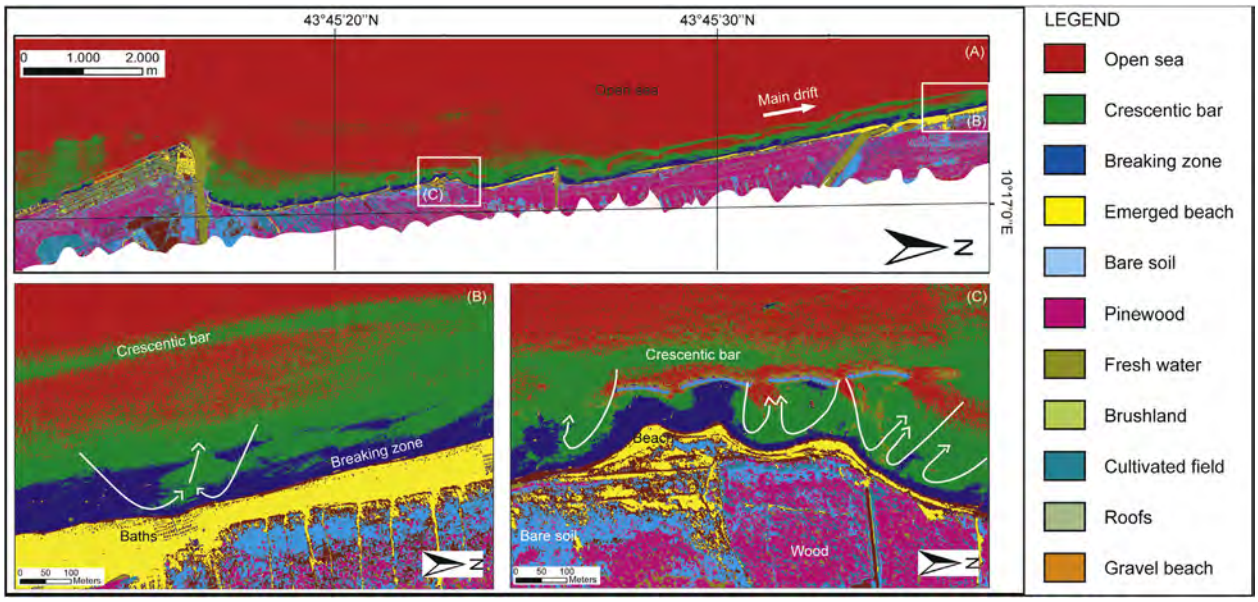


**Fig. 9.** Results of the Minimum distance classification algorithm applied to the Daedalus ATM-2 image (A) and two zoom where the hypothesized rip and longshore currents direction are reported.

The Maximum likelihood algorithm substantially confirms the results of the Minimum distance. The two algorithms show similar evaluation indexes (Table 2) and the classification maps highlight the same elements in similar way (Fig. 10).

Results of the Spectral Angle Mapper are not showed because of the very low number of classified pixels (17.33%) and the lowest indexes values (Table 2).

The PCA methods was applied considering all the available bands of the Daedalus image. Most of the variance (99.5%) is included in the first five PCs. In details PC1, which depends on both topographic information and surface albedo, explains 80.06% of the variance. Considering the visual inspection of the single produced PC images, the PC 5 image (0.45% of the variance) shows the most interesting results (Fig. 11).

In the PC 5 image (Fig. 11) the geomorphological features of the submerged beach are detectable. In particular the two sets of submerged crescentic bars can be recognized. Furthermore two areas, characterized by different spectral response, are present. The southernmost appears brightest with respect to those located at north. The boundary between these two parts corresponds with the area where the ancient dune alignments change their direction: from SW–NE to N–S (Fig. 1). This boundary probably highlight a change in the hydrodynamic conditions and turbidity which can be caused by the presence, of coastal defense structures at south, but more probably the causes of this change are natural. In fact changes in the coastal dune alignments formed before the construction of the coastal defenses that could emphasize this process.

## Discussion

The petrographic analysis evidences two different petrographic provinces within the study area: the first one is located between the Serchio river outlet to the north and Tirrenia to the south; the second one is comprised between Tirrenia and the Scolmatore river outlet. These results confirm the direction of the main littoral drift,

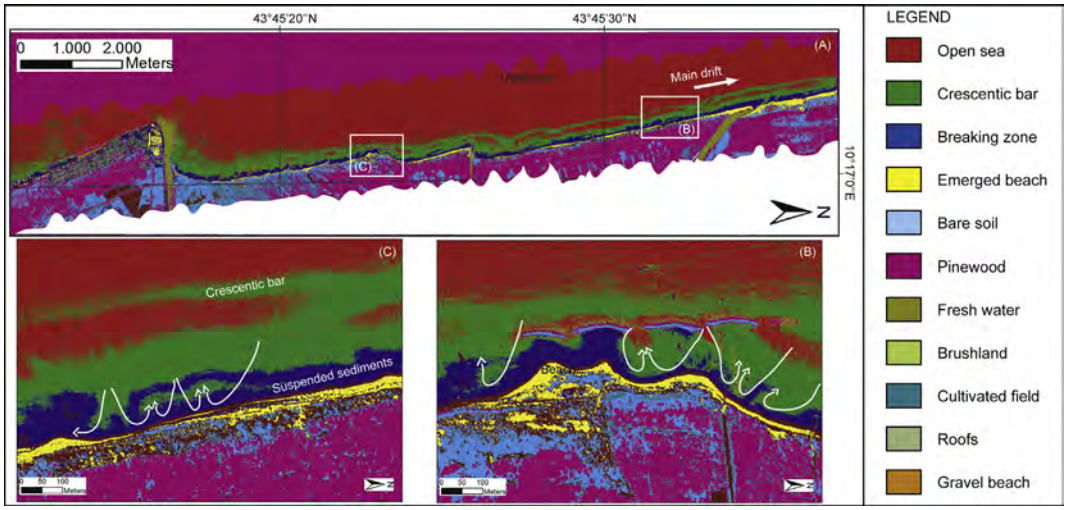


**Fig. 10.** Results of the Maximum likelihood classification algorithm applied to the Daedalus ATM-2 image (A) and two zoom where the rip and longshore currents direction are reported.

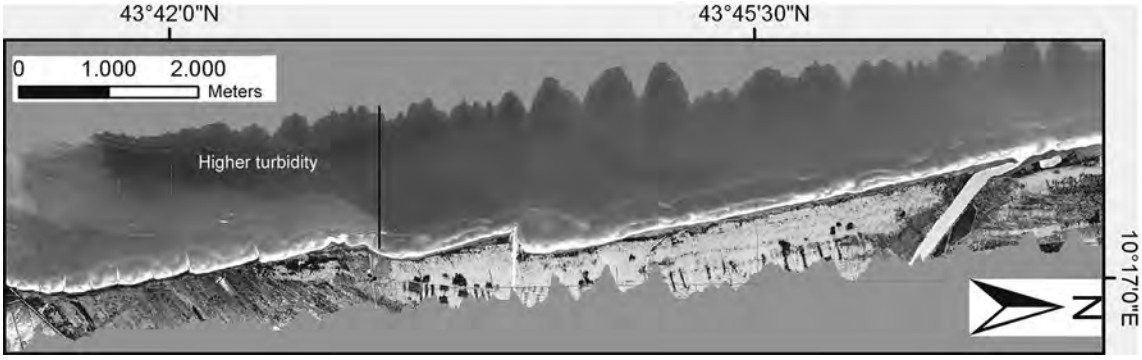


**Fig. 11.** PC 5 images of the northern sector of the study area where two areas characterized by a different spectral response can be recognized. The black line corresponds to the boundary between areas having different turbidity.

which is oriented toward the north between the Arno river and the Serchio river and between the Scolmatore canal and Tirrenia and toward the south between the Arno river and Tirrenia. The littoral drift direction highlights the presence of a convergence zone at the boundary between Tirrenia and Calambrone (Fig. 12).

Samples collected within the southern province are grouped from a statistical point of view. The PCA of the petrographic dataset clearly shows that these samples are grouped and separated from samples collected north of the Arno river outlet. Samples collected between the Arno river and the convergence zone present a more scattered distribution (Fig. 6). Also the statistical analysis highlights that the petrography of the collected samples can be used to detect the presence of two different petrographic provinces.

The difference between the detected provinces is confirmed by the grain size analysis. The southern province is characterized by the highest percentages of coarse deposits (>2 mm) and the beach sediments are better sorted. The statistical analysis of the grain size using the PC analysis shows that the most interesting variation occurs along each single sampling transect. Samples collected at −9;−10 m depth are grouped and separated from the other samples collected at different depth. In details there is a clear separation between samples collected at depth greater than −5 m and the shallower samples.

This separation can be also recognized considering the spectral characteristics of the collected samples. The PC analysis of the spectral response shows a very similar result: samples collected deeper than −5 m are statistically grouped and separated from the rest of the considered samples, suggesting that the samples spectral reflectance can be related to their grain size. This relationship is confirmed by the analysis of each spectrum of the collected samples: comparing the spectra of samples collected at 1 m and those at −9/−10 m it is evident that the deepest samples are characterized by a higher reflectance value, especially in the range between 1000 and 2500 nm. The comparison between grain size and reflectance values suggests that the latter can be affected by the amount of the medium and fine sand classes. The deepest samples are characterized by the highest percentages of find sands, on the contrary shallower samples show the lowest values both in fine sands and reflectance values. In the southern sector of the study area this distribution is inverted: the shallower samples are characterized by higher percentages of fine sands, whereas the deepest samples show higher percentages of coarse sediments (Fig. 5). This inversion is observable also in the samples spectra collected at the same depth. For example, considering the samples at 1 m (K) the highest reflectance values are recorded in the southern samples. On the contrary lower values of reflectance characterize sample collected north of the Arno river outlet, where the coarse sands class is dominant.

The results of the multispectral analysis performed on a subset of the study area using the DAEDALUS ATM-2 image, are very promising in the detection of both the sediment dispersal along the coast and the hydromorphological features. Four different algorithms were tested considering 11 different spectral classes. Parallelepiped, Minimum distance and Maximum likelihood show good performances, whereas the Spectral Angle Mapper does not provide interesting results.

These techniques allowed an accurate identification of hydromorphological forms, in particular in the submerged part of the beach located north of the Arno river outlet where several items are clearly detected. For example all the maps produced by the different algorithms highlight the fresh water input coming from the Serchio and Arno rivers, the emerged beach, the beach face besides the bare soil, the brushland and the pinewood. The most interesting results concern the submerged part of the beach. The produced maps clearly highlight the presence of a well developed crescentic bar at a distance between 150 and 370 m from the coastline.

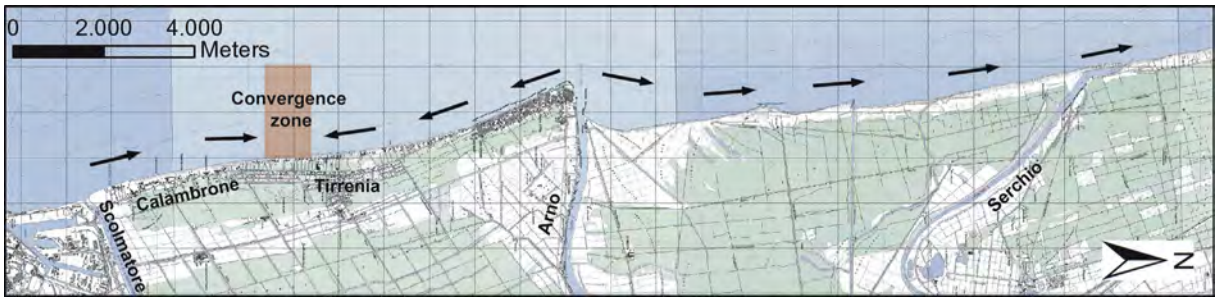


**Fig. 12.** Direction of the main littoral drift that characterizes the study area and the location of the convergence zone.

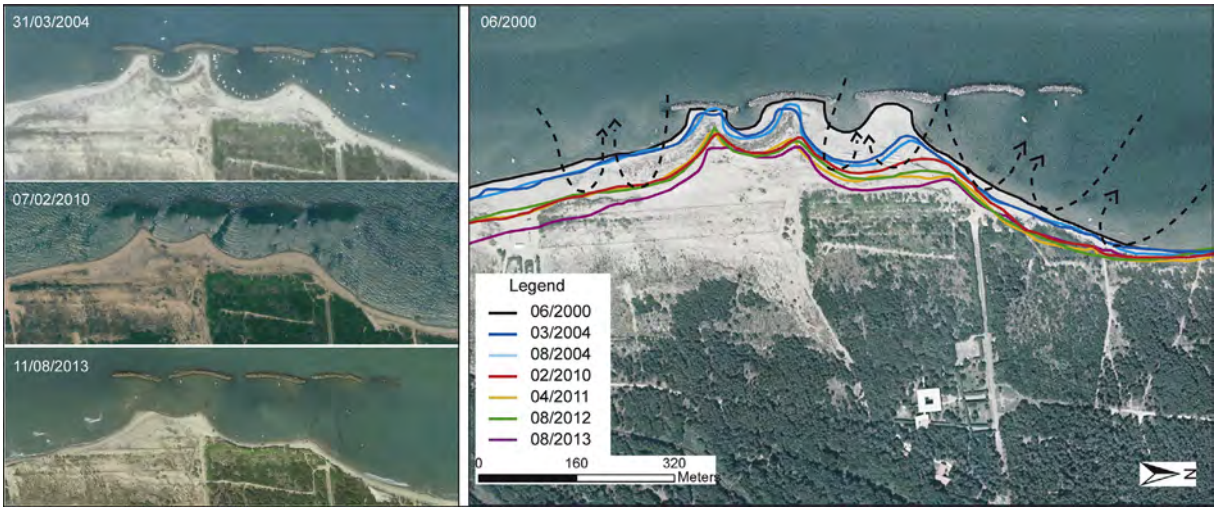


**Fig. 13.** Evolution of the coastline of a sector of the study area between the 2000 and the 2013 and the direction of the rip currents detected using the algorithms applied on the multispectral image.

The detection of the rip currents is a very important issue because of these processes represent a worldwide lethal natural hazard but also for their erosional effect. Rip currents detected using the aforementioned algorithms were compared with the areas most affected by erosional processes. The erosional effect on selected areas was measured comparing an orthophoto acquired in the 2000, five GoogleEarth images acquired in different periods, between the 2004 and the 2013 (Fig. 13) and the multispectral image acquired in the 2012.

The area corresponds to the clip C in Figs (8)–(10). The comparison among the images allowed to evaluate the evolution of the coast in the last 13 years. The retreat of the coastline is evident and reaches its maximum in correspondence with the central barrier where it is about 140 m. The areas most affected by the erosive phenomena are located in correspondence with the detected rip currents confirming the results obtained by the three considered algorithms. Results are in agreement with the classical flow-behavior of long sandy beaches (Fig. 14) (Dalrymple et al., 2011).

The identification of the areas most affected by erosional processes and the map obtained using the supervised classifications allowed the detection of several dangerous zone where rip currents are present and the evaluation of their directions. This result represent a further step in the characterization of the longshore currents within the surf zone, with respect to the traditional analysis such as the petrographic study, which allowed the identification of the main littoral drift only. The PCA performed on the Daedalus image confirms these results highlighting the presence of two areas, located north of the Arno river outlet and characterized by different hydrodynamic setting. The boundary between these two areas separates zones affected by different spatial changes of the beach. The southern sector is characterized by a loss of extent of 232.355 $m^2/m$ between the 1938 and the 2004 (Bini, Casarosa, & Ribolini, 2008) whereas the northern sector lost 170.673 $m^2/m$ in the same period.

All the presented methodologies, considering their advantages and drawbacks (Table 3), can be profitably integrated and used in the characterization and management of the coastal environment, both for its protection and preservation. The use of the only traditional techniques is very expensive for wide study areas and, usually, the sampling procedure takes time. On the contrary remote sensing techniques allow to obtain several information over wide area in a short time but they usually requires ground truth validation. The combined approach between remote sensing and

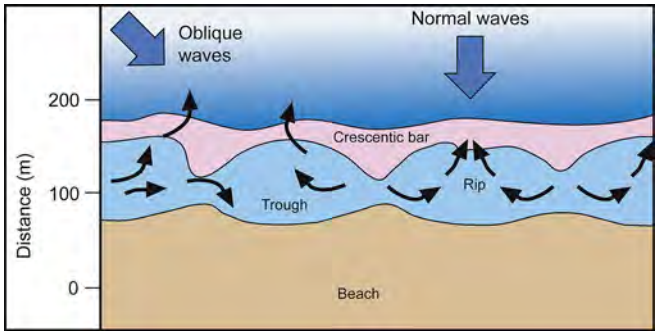


**Fig. 14.** Classic flow-behavior of rip currents in long sandy beaches subjected to normal and oblique waves. (Modified after Dalrymple et al., 2011).

**Table 3**
Advantages and drawbacks of the adopted methodologies.

| Methods | Advantages | Drawbacks |
|---|---|---|
| Traditional petrography analysis | • Detailed petrographic characterization<br>• Identification of sediment supply area | • Time and money consuming |
| Traditional grain size analysis | • Detailed grain size characterization | • Time and money consuming |
| Hyperspectral analysis (petrography) | • Time and money saving | • Difficult in detection most of the minerals |
| Hyperspectral analysis (grain size) | • Time and money saving<br>• Detection of grain size trends | • Difficult in detection of grain size classes |
| Multispectral analysis | • Time saving<br>• Detection of several morphological features<br>• Detection of several hydrodynamic features<br>• Detection of physical properties of the submerged beach | • Money consuming<br>• Needs for ground truth validation |

traditional techniques shows that high resolution remote sensing data can be easily validated using a very reduced amount of field observation (samples or field survey). Another problem is related by the fact that a high resolution image represents a snapshot of an area in an exact moment. Coastal areas are very dynamic environment where longshore and rip currents can vary during a year. A complete study of the coastal environment dynamics needs for several images acquisition in a year. This more suitable approach can sensibly increases the costs.

## Conclusion

In this work several in-situ and remote sensing techniques were used to identify beach hydro and geomorphological forms and processes in order to provide useful tools for the characterization of the coastal environment. In particular, results obtained by the classic in-situ analysis were compared to those obtained using remote sensed data acquired by hyper and multispectral sensors. The former were also used to validate the latter. The main results are:

- The study of the petrographic composition highlighted the presence of two petrographic provinces. The first is comprised between the Serchio river outlet and the Calambrone village, whereas the second is located in the southern part of the study area, between the Calambrone village and the Livorno harbor. The northern province is fed by the Arno river sediments and subordinately by the Serchio river. The southern province is influenced by the Scolmatore river.
- The spectral analysis yielded a very similar result. Samples belonging to the southern petrographic province are characterized by higher reflectance values. The groupings are particularly evident at 1 m depth. The PC analysis performed on both the grain size and the spectral datasets show that samples A (−9/−10 m) and K (1 m) clearly represent two different clusters, suggesting that grain size distribution can be spectrally detected.
- The combined use of the ASD-fieldspec portable hyperspectral sensor and the air-borne ATM-2 Daedalus multispectral sensor was useful to retrieve spectral characteristics of coastal sediments which are related to their physical properties, such as petrographic composition and grain size distribution.
- The Daedalus image was processed, using four different pixel-based classification algorithms and the PC analysis, to map the distribution of some beach geomorphological features (e.g. crescentic bar, emerged beach). The surf zone was clearly identified and, within it, areas affected by the presence of rip currents were detected. These areas are of particular interest because of their hazard for bathers and swimmers and because they are particularly affected by erosional phenomena.

This works propose an integrated approach using remote sensing and traditional techniques that will be useful for local authorities intervention in coastal areas. In particular, optical remote sensing technique can be profitably used in the characterization of coastal currents (longshore and rip) reducing the use of conventional analysis which are usually time and money consuming. The obtained results can be profitably used for a proper management of coastal areas allowing to plan intervention aimed at contrasting beach erosion phenomena.

We suggest further remote sensing based studies. The obtained results are encouraging to insist in the investigation of the spectral behavior of littoral sands, in order to understand how the lithological composition affects the spectral behavior and possibly to draw robust conclusions on coastal dynamics.

An airborne routine acquisition of multispectral images (multi temporal analysis) could allow to detect changing in the longshore and/or rip currents direction during the year. A multi temporal analysis can be also used to constantly monitor the effect of the erosional processes along the coast.

Furthermore these images can be also used to update high resolution land use maps and land use change products, to assess of salinity impacts on agriculture and natural ecosystems located along the coast.

## Acknowledgments

We thank the Provincia di Pisa which provided the results of the petrographic and grain size analysis. The DAEDALUS Airborne Thematic Mapper (ATM-2) multispectral image was provided by the AGEA/TELAER STA© within the framework of the Daedalus-Telear Announcement of Opportunity “Utilizzo di dati telerilevati per lo studio della dispersione dei sedimenti lungo la costa pisana” (Scientific Responsibility: A. Ciampalini). FeDiT is supported by a post-doc fellowship founded by the Regione Toscana (UNIPI-FSE) under the project RADSAFE (UNIPI-4) in the framework of the research agreement between DST-UNIPI, DST-UNIFI and Ellegi s.r.l. – LiSALab.

## References

Abd El-Kawy, O. R., Rød, J. K., Ismail, H. A., & Suliman, A. S. (2011). Land use and land cover change detection in the western Nile delta of Egypt using remote sensing data. *Applied Geography, 31*, 483–494.

Abdi, H., & Williams, L. J. (2010). Principal component analysis. *Wiley Interdisciplinary Reviews: Computational Statistics, 2*, 433–459.

Aiello, E., Bartolini, C., Caputo, C., D'Alessandro, L., Fanucci, F., Fierro, G., et al. (1976). *Bollettino della Società Geologica Italiana, 94*, 1519–1571.

Aminti, P. L., & Pranzini, E. (2000). Indagine sperimentale per la ristrutturazione delle difese di Marina di Pisa. *Studi Costieri, 3*, 57–70.

Amorosi, A., Rossi, V., Sarti, & Mattei, R. (2013). Coalescent valley fills from the late quaternary record of Tuscany (Italy). *Quaternary International, 288*, 129–138.

Anil Ari, H., Yüksel, Y., Özkan Çevic, E., Güler, A., Yalçiner, C., & Bayram, B. (2007). Determination and control of longshore sediment transport: a case study. *Ocean Engineering, 34*, 219–223.

Baily, B., & Nowel, D. (1996). Techniques for monitoring coastal change: a review and case study. *Ocean and Coastal Management, 32*, 85–95.

Bertoni, D., Grottoli, E., Ciavola, P., Sarti, G., Benelli, G., & Pozzebon, A. (2013). On the displacement of marked pebbles on two-clastic beaches during short air-weather periods (Marina di Pisa and Portonovo, Italy). *Geo-Marine Letters, 33*, 463–476.

Bertoni, D., & Sarti, G. (2011). On the profile evolution of three artificial pebble beaches at Marina di Pisa, Italy. *Geomorphology, 130*, 244–254.

Bertoni, D., Sarti, G., Benelli, G., Pozzebon, A., & Raguseo, G. (2010). Radio Frequency Identification (RFID) technology applied to the identification of underwater and subaerial coarse sediment movement. *Sedimentary Geology, 228*, 140–150.

Bertoni, D., Sarti, G., Benelli, G., Pozzebon, A., & Raguseo, G. (2012). Transport trajectories of “smart” pebbles on an artificial coarse-grained beach at Marina di Pisa (Italy): implications for beach morphodynamics. *Marine Geology, 291*, 227–235.

Bini, M., Casarosa, N., & Ribolini, A. (2008). L'evoluzione diacronica della linea di riva del litorale pisano (1938-2004) sulla base del confronto di immagini aeree georeferenziate. *Atti della Società Toscana di Scienze Naturali – Memorie Serie A, 113*, 1–12.

Borges, J., & Huh, Y. (2007). Petrography and chemistry of the bed sediments of the Red River in China and Vietnam: provenance and chemical weathering. *Sedimentary Geology, 194*, 119–156.

Brenton, R. G. (2003). *Chemometrics: Data analysis for the laboratory and chemical plant*. Chirchester, UK: John Wiley & Sons, 504 pp.

Chauvaud, S., Bouchon, C., & Maniere, R. (1998). Remote sensing techniques adapted to high resolution mapping of tropical coastal marine ecosystem (coral reefs, seagrass beds and mangrove). *International Journal of Remote Sensing, 19*(18), 3625–3639.

Ciampalini, A., Consoloni, I., & Sarti, G. (2011). Fault array evolution in extensional basins: insight from statistical analysis of gravel deposits in the Cecina River (Tuscany, Italy). *Sedimentology, 58*, 1895–1913.

Ciampalini, A., Garfagnoli, F., Antonielli, B., Del Ventisette, C., & Moretti, S. (2012). Photo-lithological map of the southern flank of the Tindouf Basin (Western Sahara). *Journal of Maps, 8*(4), 453–464.

Ciampalini, A., Garfagnoli, F., Antonielli, B., Moretti, S., & Righini, G. (2013). Remote sensing techniques using Landsat ETM+ applied to the detection of iron ore deposits in Western Africa. *Arabian Journal of Geosciences, 6*, 4529–4546.

Cipriani, L. E., Ferri, S., Iannotta, P., Paolieri, F., & Pranzini, E. (2001). Morfologia e dinamica dei sedimenti del litorale della Toscana settentrionale. *Studi Costieri, 4*, 119–156.
Congalton, R. G., & Mead, R. A. (1983). A quantitative method to test for consistency and correctness in photointerpretation. *Photogrammetric Engineering and Remote Sensing, 49*, 69–74.
Dalrymple, R. A., MacMahan, J. H., Reniers, J. H. M., & Nelko, V. (2011). Rip currents. *Annual Review of Fluid Mechanics, 43*, 551–581.
Dharmaratne, G. S., & Braithwaite, A. E. (1998). Economic valuation of the coastline for tourism in Barbados. *Journal of Travel Research, 37*(2), 138–144.
Dickinson, W. R. (1970). Interpreting detrital modes of graywacke and arkose. *Journal of Sedimentary Petrology, 40*, 695–707.
Dickinson, W. R., & Suckzek, C. A. (1979). Plate tectonics and sandstone compositions. *Bulletin of American Association of Petroleum Geologist, 63*, 2164–2182.
El Mrini, A., Maanan, M., Anthony, E. J., & Taaouati, M. (2012). An integrated approach to characterize the interaction between coastal morphodynamics, geomorphological setting and human interventions on the Mediterranean beaches of northwestern Morocco. *Applied Geography, 35*, 334–344.
Gandolfi, G., & Paganelli, L. (1975). Il litorale pisano-versiliese (area campione Alto Tirreno); composizione, provenienza e dispersione delle sabbie. *Bollettino della Società Geologica Italiana, 94*, 1273–1295.
Garfagnoli, F., Ciampalini, A., Moretti, S., Chiarantini, L., & Vettori, S. (2013). Quantitative mapping of clay minerals using airborne imaging spectroscopy: new data on Mugello (Italy) from SIM-GA prototypal sensor. *European Journal of Remote Sensing, 46*, 1–17.
Garfagnoli, F., Martelloni, G., Ciampalini, A., Innocenti, L., & Moretti, S. (2013). Two GUIs-based analysis tool for spectroradiometer data pre-processing. *Earth Science Informatics, 6*(4), 227–240.
Gazzi, P. (1966). Le arenarie del flysch supracretaceo dell'Appennino Modenese: correlazioni con il flysch di Monghidoro. *Mineralogica et Petrographica Acta, 12*, 69–97.
Graham, S. A., Ingersoll, R. V., & Dickinson, W. R. (1976). Common provenance for lithic grains in carboniferous sandstones from Ouachita mountains and black warrior basin. *Journal of Sedimentary Petrology, 46*, 620–632.
Holman, R., & Haller, M. C. (2013). Remote sensing of nearshore. *Annual Review of Marine Science, 5*, 95–113.
Ingersoll, R. V., Bullard, T. F., Ford, R. L., Grimm, J. P., Pickle, J. D., & Sares, S. W. (1984). The effects of grain size on detrital modes: a test of the Gazzi-Dickinson point counting method. *Journal of Sedimentary Petrology, 54*, 103–116.
Isaaks, E. H., & Srivastava, R. M. (1989). *Applied geostatistics*. New York: Oxford University Press.
Khaleghi, M., Ranjbar, H., Shahabpour, J., & Honarmand, M. (2014). Spectral angle mapping, spectral information divergence, and principal component analysis of the ASTER SWIR data for exploration of porphyry copper mineralization in the Sarduiyeh area, Kerman province, Iran. *Applied Geomatics, 6*(1), 49–58.
Kruse, F. A., Lefkoff, A. B., Boardman, J. B., Heidebrecht, K. B., Shapiro, A. T., Barloon, P. J., et al. (1993). The spectral image processing system (SIPS) – interactive visualization and analysis of imaging spectrometer data. *Remote Sensing of Environment, 44*, 145–163.
Kuenzer, C., van Beijima, S., Gessner, U., & Dech, S. (2014). Land surface and environmental challenges of the Niger Delta, Africa: remote sensing-based analyses spanning three decades (1986–2013). *Applied Geography, 53*, 354–368.
Li, J., & Chen, W. (2005). A rule-based method for mapping Canada's wetlands using optical, radar and DEM data. *International Journal of Remote Sensing, 26*(22), 5051–5069.
Liew, S. C., Chang, C. W., & Kwoh, L. K. (2012). International archives of the Photogrammetry, Remote Sensing and Spatial Information Sciences. *Sensitivity analysis in the retrieval of turbid coastal water bathymetry using worldview-2 satellite data* (Vol. XXXIX-B7). Melbourne, Australia: XXII ISPRS Congress.
Liu, Y., Islam, M. A., & Gao, J. (2003). Quantification of shallow water quality parameters by means of remote sensing. *Progress in Physical Geography, 27*, 24–43.
Loughlin, W. P. (1991). Principal component analysis for alteration mapping. *Photogrammetric Engineering and Remote Sensing, 57*, 1163–1169.
Lushine, J. B. (1991). A study of rip current drownings and related weather factors. *National Weather Digest, 16*, 13–19.
Manning, R., Wang, B., Valliere, W., Lawson, S., & Newman, P. (2002). Research to estimate and manage carrying capacity of a tourist attraction: a study of Alcatraz Island. *Journal of Sustainable Tourism, 10*(5), 388–403.
Mc Kenna, J., O'Hagan, A. M., Power, J., Macleod, M., & Cooper, A. (2007). Coastal dune conservation on an Irish commonage: community-based management or tragedy of the commons? *The Geographical Journal, 173*(2), 157–169.
Molinaroli, E., Sarretta, A., Ferrarin, C., Masiero, E., Specchiulli, A., & Guerzoni, S. (2014). Sediment grain size and hydrodynamics in Mediterranean coastal lagoons: Integrated classification of abiotic parameters. *Journal of Earth System Science, 123*(5), 1097–1114.
Power, H. E., Holman, R. A., & Baldock, T. E. (2011). Swash zone boundary conditions derived from optical remote sensing of swash zone flow patterns. *Journal of Geophysical Research, 116*(6). C06007.
Pranzini, E. (1983). Studi di morfologia costiera: l'erosione del delta dell'Arno. *Quaderni del Museo di Storia Naturale di Livorno, 4*, 7–18.
Pranzini, E. (1989). A model for cuspidate delta erosion. *Coastal Zone, 89*, 4345–4357.
Pranzini, E. (2004). Caratteristiche morfologiche e sedimentologiche di una zona di convergenza del trasporto litoraneo (Versilia, Toscana). *Studi Costieri, 8*, 135–149.
Pu, R., & Bell, S. (2013). A protocol for improving mapping and assessing of seagrass abundance along the west central coast of Florida using Landsat TM and EO-1 ALI/Hyperion images. *Remote Sensing of Environment, 83*, 116–129.
Raiber, M., White, P. A., Daughney, C. J., Tschritter, C., Davidson, P., & Bainbridge, S. E. (2012). Three-dimensional geological modelling and multivariate statistical analysis of water chemistry data to analyse and visualise aquifer structure and groundwater composition in the Wairau Plain, Marlborough District, New Zealand. *Journal of Hydrology, 436–437*, 13–34.
Rapetti, F., & Vittorini, S. (1974). Osservazioni sulla variazione dell'ala destra del delta dell'Arno. *Atti della Società Toscana di Scienze Naturali – Memorie Serie A, 81*, 25–88.
Richards, J. A. (1999). *Remote sensing digital image analysis*. Berlin: Springer–Verlag.
Rozenstein, O., & Karnieli, A. (2011). Comparison of methods for land-use classification incorporating remote sensing and GIS inputs. *Applied Geography, 31*, 533–544.
Shaw, P. J. (2003). *Multivariate statistics for the environmental sciences*. Chirchester, UK: John Wiley & Sons, 223 pp.
Shaw, W. S., Goff, J., Brander, R., Walton, T., Roberts, A., & Sherker, S. (2014). Surviving the surf zone: towards more integrated rip current geographies. *Applied Geography, 54*, 54–62.
Short, A. D., & Hogan, C. L. (1994). Rip currents and beach hazards: their impact on public safety and implications for coastal management. *Journal of Coastal Research*, 197–209. Special Issue 12, Coastal Hazards: Perception, susceptibility and mitigation.
Small, C., Steckler, M., Seeber, L., Akhter, S. H., Goodbred, S., Jr., Mia, B., et al. (2009). Spectroscopy of sediments in the Ganges–Brahmaputra delta: spectral effects of moisture, grain size and lithology. *Remote Sensing of Environment, 113*, 342–361.
Smits, P. C., Dellepiane, S. G., & Schowengerdt, R. A. (1999). Quality assessment of image classification algorithms for land-cover mapping: ma review and proposal for a cost-based approach. *International Journal of Remote Sensing, 20*, 1461–1486.
Stehman, S. V. (1996). Estimating the Kappa coefficient and its variance under stratified random sampling. *Photogrammetric Engineering and Remote Sensing, 62*, 401–407.
Stojanovic, T. A., & Ballinger, R. C. (2009). Integrated coastal management: a comparative analysis of four UK initiatives. *Applied Geography, 29*, 49–62.
Teodoro, A., Pais-Barbosa, J., Gonçalves, H., Veloso-Gomes, F., & Taveira-Pinto, F. (2011). Identification of beach hydromorphological patterns/forms through image classification techniques applied to remotely sensed data. *International Journal of Remote Sensing, 32*(22), 7399–7422.
Teodoro, A., Pais-Barbosa, J., Veloso-Gomes, F., & Taveire-Pinto, F. (2009). Evolution of beach hydromorphological behaviour and classification using image classification techniques. *Journal of Coastal Research, 56*, 1607–1611.
Winter, T. C., Mallroy, S. E., Allen, T. R., & Rosenberry, D. O. (2000). The use of principal component analysis for interpreting ground water hydrographs. *Ground Water, 38*(2), 234–246.
Xu, J., Zhang, Z., Zhao, X., Wen, Q., Zuo, L., Wang, X., et al. (2014). Spatial and temporal variations of coastlines in northern China. *Journal of Geographical Sciences, 24*, 18–32.
Zacarias, D. A., Williams, A. T., & Newton, A. (2011). Recreation carrying capacity estimations to support beach management at Praia de Faro, Portugal. *Applied Geography, 31*, 1075–1081.
Zuffa, G. G. (1980). Hybrid arenites: their composition and classification. *Journal of Sedimentary Petrology, 50*, 21–29.
Zuffa, G. G. (1985). Optical analyses of arenites: influence of methodology on compositional results. In G. G. Zuffa (Ed.), *Provenance of arenites. NATO-ASI* (pp. 165–189). Dordrecht: Reidel Publ. Co.